An Overcomplete Stitching Algorithm for Time Decoding Machines

Aurel A. Lazar, *Fellow, IEEE*, Ernö K. Simonyi, and László T. Tóth

***Abstract*—We investigate a class of finite-dimensional time decoding algorithms that: 1) is insensitive with respect to the time-encoding parameters; 2) is highly efficient and stable; and 3) can be implemented in real time. These algorithms are based on the observation that the recovery of time encoded signals given a finite number of observations has the property that the quality of signal recovery is very high in a reduced time range. We show how to obtain a local representation of the time encoded signal in an efficient and stable manner using a Vandermonde formulation of the recovery algorithm. Once the signal values are obtained from a finite number of possibly overlapping observations, the reduced-range segments are stitched together. The signal obtained by segment stitching is subsequently filtered for improved performance in recovery. Finally, we evaluate the complexity of the algorithms and their computational requirements for real-time implementation.**

***Index Terms*—Asynchronous communications, frames, irregular sampling, real-time stitching algorithms, time decoding machines (TDMs), time encoding machines (TEMs).**

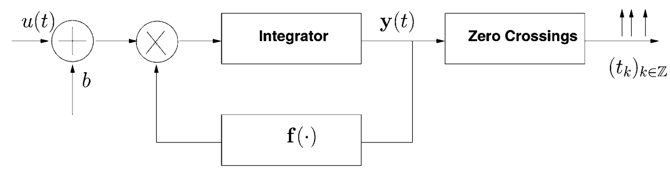

Fig. 1. TEM with multiplicative coupling.

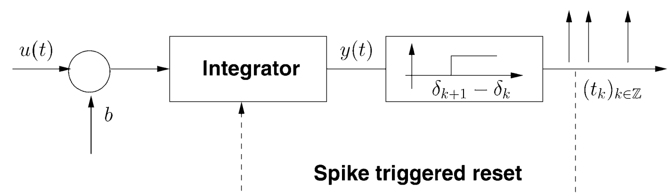

Fig. 2. IAF neuron with variable threshold.

I. Introduction

TIME encoding [12] is a real-time asynchronous mechanism of mapping the amplitude of a bandlimited signal $u(t)$, $t \in \mathbb{R}$, into a strictly increasing time sequence (t_k), $k \in \mathbb{Z}$, where $\mathbb{R}$ and $\mathbb{Z}$ denote the sets of real numbers and integers, respectively. A time encoding machine (TEM) is the realization of an *asynchronous* time encoding mechanism. A time decoding machine (TDM) is the realization of an algorithm for signal recovery with arbitrary accuracy.

The interest in time encoding in signal processing is driven by the expected paradigm shift in the design and implementation of future analog to digital converters from information representation in the *amplitude domain* to information representation in the *time domain*. Due to the ever decreasing size of integrated circuits and the attendant low-voltage, amplitude-domain high-precision quantizers are more and more difficult to implement. TEMs leverage the phenomenal device speeds that a temporal code can take advantage of [18]. The interest in temporal encoding in neuroscience is closely linked with the natural representation of sensory stimuli (signals) as a sequence of action potentials (spikes). Spikes are discrete time events that carry information about stimuli.

A general class of TEMs that exhibit multiplicative coupling, and, feedforward and feedback was introduced in [15]. The basic underlying circuit consists of a garden variety oscillator whose output feeds a zero crossings detector (see Fig. 1). The detector generates the time sequence of the zeros of the oscillator waveform. The oscillator is in turn modulated by an input bandlimited signal. The analysis in [15] demonstrated that TEMs with multiplicative coupling are I/O equivalent with simple nonlinear circuits. The TEM shown in Fig. 1 is input–output (I/O) equivalent with an integrate-and-fire (IAF) neuron with variable threshold depicted in Fig. 2. The variable threshold sequence is given by the difference between the consecutive zeros of the waveform generated by the oscillator for unit input. The same result holds for a TEM with feedforward while a TEM with feedback (see Fig. 3) is I/O equivalent with an asynchronous sigma–delta modulator (see Fig. 4) with variable thresholds [15].

For all TEMs considered, the bandlimited signal at the input can be perfectly recovered from the zero crossings of the modulated signal and the threshold sequence. Perfect reconstruction can be achieved provided that a Nyquist-type rate condition is satisfied. Although methods used in frame theory [3], [11] and irregular sampling [4], [20] are needed to establish these conditions [12], [13], the algorithms are often easy to find and only

Manuscript received June 07, 2007; revised November 10, 2007 and February 11, 2008. First published March 21, 2008; current version published October 29, 2008. This work was supported in part by the National Science Foundation under Grant CCF-06-35252 (AAL) and in part by the National Office for Research and Technology (NKTH Hungary) as part of the project *Time-encoded Asynchronous Mobile Communications for Development of Integrated Monitoring Systems*, INTMON05 (EKS and LTT). This paper was recommended by Associate Editor B. C. Levy.

A. A. Lazar is with the Department of Electrical Engineering, Columbia University, New York, NY 10027 USA (e-mail: aurel@ee.columbia.edu).

E. K. Simonyi is with Ministry of Defense Electronics, Logistic and Property Management Company, Budapest 1101, Hungary (e-mail: simonyi.erno@hmei.hu).

L. T. Tóth is with the Department of Telecommunications and Media Informatics, Budapest University of Technology and Economics, Budapest 1111, Hungary (e-mail: tothl@tmit.bme.hu).

Digital Object Identifier 10.1109/TCSI.2008.920982

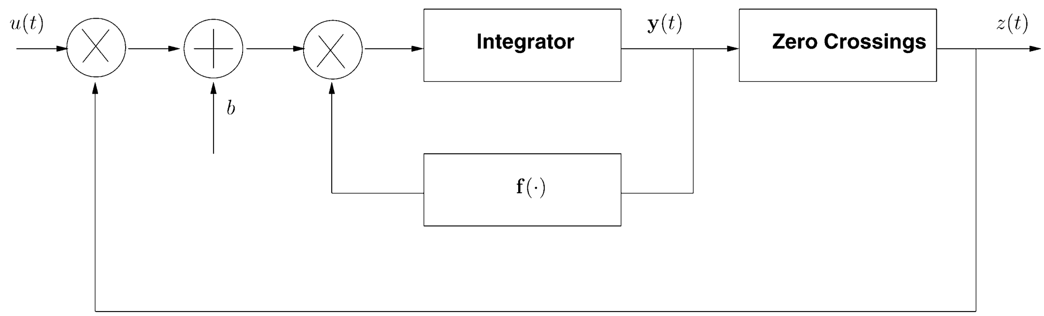

Fig. 3. TEM with multiplicative coupling and feedback.

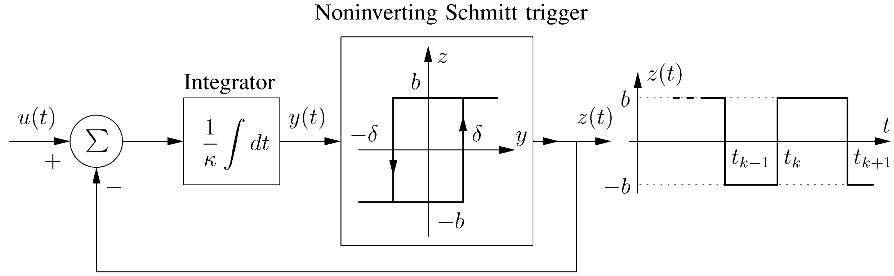

Fig. 4. TEM realized as an asynchronous sigma–delta modulator with $2\kappa\delta = \delta_{k+1} - \delta_k$, $k \in \mathbb{Z}$.

require solving a consistent but (typically) ill-conditioned infinite-dimensional system of linear equations.

In this paper we investigate an algorithm for signal recovery that uses an overlapping sequence of finite-dimensional coverings of the infinite-dimensional system. The algorithm: 1) is insensitive with respect to the TEM parameters; 2) is highly efficient and stable; and 3) can be implemented in real time. It is based on the observation that the recovery of time encoded signals given a finite number of observations has the property that the quality of signal recovery is very high in a reduced time range. A similar time-locality property was investigated in [5] in the context of irregular sampling. We show how to obtain a local representation of the time-encoded signal in an efficient and stable matter using a Vandermonde formulation of the recovery algorithm. Once the signal values are obtained from a finite number of possibly overlapping observations, the reduced-range segments are stitched together. The signal obtained by segment stitching is finally filtered for improved performance in recovery.

The recovery of time encoded bandlimited signals is closely related to the recovery of bandlimited signals from irregular samples. In [21] an extensive numerical analysis of algorithms for signal recovery from irregular samples was presented; in addition, extensive performance results for the case when the number of samples is large were discussed. These algorithms, however, do not operate in real-time. In order to address the real-time requirements, we have explored in the past efficient stitching algorithms [16] using a pseudo-inverse formulation of local recovery. However, the latter algorithms are parameter sensitive and exhibit stability issues. In contrast, the algorithms presented here are parameter-insensitive and have provably robust stability properties.

The outline of the paper is as follows. Section II describes a general class of TEMs with multiplicative coupling and the corresponding TDMs that achieve perfect signal recovery. Finite-dimensional TDMs are described in Section III. Section III.B gives a parameter-insensitive and minimum-least square formulation for signal recovery including estimates for the reconstruction error. Section IV provides an overcomplete stitching algorithm for the overall signal reconstruction in real-time as well as overall error estimates. Practical computational considerations are dealt with in Section V. Two examples are given that evaluate the theoretical results.

II. TDMS ACHIEVING PERFECT SIGNAL RECOVERY

A. TEMs With Multiplicative Coupling

As already mentioned, the TEM with multiplicative coupling shown in Fig. 1 is I/O equivalent [15] with an IAF neuron with the variable threshold sequence $\delta_{k+1} - \delta_k$ depicted in Fig. 2. The sequence $(\delta_k), k \in \mathbb{Z}$, represents the set of zeros of the oscillator waveform in Fig. 1. The analytical characterization of the IAF neuron is given by

$$\int_{t_k}^{t_{k+1}} u(s)ds = \delta_{k+1} - \delta_k - b(t_{k+1} - t_k) \tag{1}$$

where $u = u(t), t \in \mathbb{R}$, is the TEM input signal and $(t_k), k \in \mathbb{Z}$, is the output time sequence. The elements of the time sequence will also be referred to as trigger times. The input signal is assumed to be bounded in amplitude

$$|u(t)| \leq c < b \tag{2}$$

has finite energy on $\mathbb{R}$ and is bandlimited to $[-\Omega, \Omega]$.

An example of a TEM with multiplicative coupling and feedback is shown in Fig. 3. This circuit is I/O equivalent with the asynchronous sigma–delta modulator (ASDM) (an example is shown in Fig. 4) that is analytically described by

$$\int_{t_k}^{t_{k+1}} u(s)ds = (-1)^k[\delta_{k+1} - \delta_k - b(t_{k+1} - t_k)] \quad (3)$$

with $y(t_0) = -(\delta_1 - \delta_0)$. Equation (1) and (3) are instances of the t-transform [12]. They map the amplitude information contained in the bandlimited signal $u = u(t), t \in \mathbb{Z}$, into the increasing time sequence $(t_k), k \in \mathbb{Z}$.

B. Time Decoding Machines

In what follows we shall assume that the class of TEMs under consideration are I/O equivalent with a nonlinear circuit with input $u(t), t \in \mathbb{R}$, and output $(t_k), k \in \mathbb{Z}$, that satisfies the t-transform

$$\int_{t_k}^{t_{k+1}} u(s)ds = q_k \quad (4)$$

where q_k is a function of t_k and t_{k+1} with $t_{k+1} > t_k$, $k \in \mathbb{Z}$. Note that the q_k's in the (1) and (3) are linear functions of t_k and t_{k+1} for the IAF neuron and ASDM described above. See [15] for an example of nonlinear functions $q_k, k \in \mathbb{Z}$.

Theorem 1 [12], [15]: If the Nyquist-type rate condition

$$\max_k T_k < \frac{\pi}{\Omega} \quad \text{where } T_k = t_{k+1} - t_k \quad (5)$$

is satisfied, the bandlimited input signal $u = u(t), t \in \mathbb{R}$, can be recovered as

$$u(t) = \sum_{\ell \in \mathbb{Z}} c_\ell g(t - s_\ell) \quad (6)$$

where $s_\ell = (t_\ell + t_{\ell+1})/2$ and

$$g(t) = \frac{\sin(\Omega t)}{\pi t} \quad (7)$$

is the impulse response of an ideal low-pass filter (LPF) with cutoff frequency Ω. The set of coefficients $c_\ell, \ell \in \mathbb{Z}$, satisfy the system of linear equations

$$\sum_{\ell \in \mathbb{Z}} \underbrace{c_\ell}_{[\mathbf{c}]_\ell} \underbrace{\int_{t_k}^{t_{k+1}} g(s - s_\ell)ds}_{[\mathbf{G}]_{k\ell}} = \underbrace{q_k}_{[\mathbf{q}]_k} \quad (8)$$

for all $k \in \mathbb{Z}$. Finally, the matrix $\mathbf{G}$, vectors $\mathbf{q}$ and $\mathbf{c}$ introduced above, verify the linear equation

$$\mathbf{G}\mathbf{c} = \mathbf{q}. \quad (9)$$

Without loss of generality, our discussion will focus on TEMs realized as ASDMs (an example is shown in Fig. 4). We have extensively investigated the latter circuit both by simulations [10] and experimentally [9]. We note that, parameter-insensitive TDMs eliminate the effects of several circuit imperfections that are beyond the ideal TEM model of Fig. 4, [10].

III. Finite-Dimensional TDMS

A. Class of Finite-Dimensional Recovery Algorithms

In what follows we shall consider the covering sequence $[t_i, t_{i+N}], i \in \mathbb{Z}$, of the real line $\mathbb{R}$, where N is an arbitrary positive integer. Our first goal is to develop an accurate reconstruction for $u(t)$ for all $t \in [t_{i+M}, t_{i+N-M}]$, for given integers i, $N > 1$, and $0 < M < N/2$. $[t_{i+M}, t_{i+N-M}]$ is said to be the restricted range.

Similarly to the approach of [4] and [14], we approximate $u(t)$ on $[t_i, t_{i+N}]$ by the periodic bandlimited signal

$$u_i(t) = \sum_{n=0}^{N} j\left(\Omega - n\frac{2\Omega}{N}\right) d_{i,n} e^{j(-\Omega + n\frac{2\Omega}{N})t}. \quad (10)$$

Here $d_{i,n}$ is a set of coefficients whose values are to be determined. The bandwidth and the period of $u_i(t)$ are Ω and $2N\pi/\Omega$ (for $N \geq 1$), respectively.

The approximation in (10) can be obtained by noting that the function $v_i(t)$ defined by

$$v_i(t) = \int_t^{t_{i+N+1}} u(s)ds$$

is interpolated by

$$p_i(t) = \sum_{n=0}^{N} d_{i,n} e^{j(-\Omega + n\frac{2\Omega}{N})t}$$

as $v_i(t_{i+k}) = p_i(t_{i+k})$ for all $k = 0, 1, \ldots, N$. Since $dv_i(t)/dt = -u(t)$, $u(t)$ is approximated by $-dp_i(t)/dt$. Note that

$$\begin{aligned} v_i(t_{i+k}) &= \int_{t_{i+k}}^{t_{i+N+1}} u(s)ds \\ &= \sum_{\ell=i+k}^{i+N} \int_{t_\ell}^{t_{\ell+1}} u(s)ds \\ &= \sum_{\ell=i+k}^{i+N} q_\ell \end{aligned}$$

for all $k = 0, 1, \ldots, N$. Note also that the Dirichlet kernel above [4] is the working kernel and not $g(t)$ in (7).

Proposition 1: The coefficients $[\mathbf{d}_i]_n = d_{i,n}$ satisfy the matrix equation

$$\mathbf{V}_i \mathbf{d}_i = \mathbf{D}_i \mathbf{P} \mathbf{q}_i \quad (11)$$

for all $i \in \mathbb{Z}$, where $[\mathbf{V}_i]_{nm} = e^{jm2\Omega t_{i+n}/N}$ is a Vandermonde matrix, $\mathbf{D}_i = \mathrm{diag}(e^{j\Omega t_{i+n}})$ is a diagonal matrix, $\mathbf{P}$ is an upper triangular matrix with values $[\mathbf{P}]_{nm} = 1$ and $[\mathbf{P}]_{nm} = 0$ for $n < m + 1$ and $n \geq m + 1$, respectively, and $[\mathbf{q}_i]_n = q_{i+n}$, $n, m = 0, \ldots, N$.

Proof: The matrix (11) is a compact notation of the linear systems of equations $v_i(t_{i+k}) = p_i(t_{i+k})$ where $k = 0, 1 \ldots, N$, and $i \in \mathbb{Z}$. □

It is known [8] that $\mathbf{V}_i$ is nonsingular if $e^{j2\Omega t_{i+n}/N} \neq e^{j2\Omega t_{i+m}/N}$ for $n \neq m$. This condition is satisfied since $t_{k+1} > t_k$. Note that with (5) $2\Omega t_{i+N}/N - 2\Omega t_i/N \leq (2\Omega/N)N \max_i T_i < 2\pi$. As a result, the values of $e^{j2\Omega t_{i+n}/N}$ for all $n = 0, 1 \ldots, N$, are distinct and located within one period 2π of the complex exponential. The Vandermonde system in (11) can be solved for $\mathbf{d}_i$ by the Björk-Pereyra algorithm in a numerically very stable way with $5N^2/2$ flops [1], [8]. For convenience, it is given below.

Algorithm 1: Let $z_n^m = e^{jm2\Omega t_{i+n}/N}$ where $n, m = 0, 1, \ldots, N$, and $\mathbf{b} = \mathbf{D}_i \mathbf{P} \mathbf{q}_i$. The system of $N+1$ linear (11) can be solved with $5N^2/2$ flops as follows:

$$
\begin{aligned}
&\text{for } n = 0, \ldots, N-2 \text{ do :}\\
&\text{for } m = N, \ldots, n+1 \text{ do :}\\
&\quad b_m = (b_m - b_{m-1})/(z_m - z_{m-n-1})\\
&\text{for } n = N-2, \ldots, 0 \text{ do :}\\
&\text{for } m = n, \ldots, N-2 \text{ do :}\\
&\quad b_m = b_m - b_{m+1} z_n.
\end{aligned}
$$

At the end of the procedure $\mathbf{d}_i = \mathbf{b}$.

With this approach our numerical experiments were similar to those of [16], [14]: increasing N the accuracy of the reconstruction improves, that is, the error

$$\tilde{e}_i(t) = u(t) - u_i(t) \tag{12}$$

decreases. However, the conditioning of the system gets worse. As a consequence of Gautschi's classic results [6]–[8], estimates for $\mathcal{K}_\infty(\mathbf{V}_i)$, the infinite-norm condition number of $\mathbf{V}_i$, are given by the following lemma.

Lemma 1:

$$
\begin{aligned}
&\frac{N+1}{2^N S_i} < \mathcal{K}_\infty(\mathbf{V}_i) \leq \frac{N+1}{S_i}\\
&S_i = \min_{0 \leq n \leq N} \prod_{\substack{m=0\\ m \neq n}}^{N} |\sin(\Omega(t_{i+n} - t_{i+m})/N)|.
\end{aligned} \tag{13}
$$

Proof: The definition of ∞-norm of $\mathbf{V}_i$ gives:

$$\| \mathbf{V}_i \|_\infty = \max_{0 \leq n \leq N} \sum_{m=0}^{N} |e^{jm2\Omega t_{i+n}/N}| = N + 1. \tag{14}$$

Let $\mathbf{V}$ be an N by N Vandermonde matrix generated by the arbitrary distinct nodes z_n as $[\mathbf{V}]_{n\ell} = z_n^\ell$ where $\ell, n = 1, \ldots, N$. The lower bound [6] and the upper bound [7] for $\| \mathbf{V}^{-1} \|_\infty$ are given by

$$\max_{0 \leq n \leq N} \prod_{\substack{m=0\\ m \neq n}}^{N} \frac{\max(1, |z_m|)}{|z_n - z_m|}$$

and

$$\max_{0 \leq n \leq N} \prod_{\substack{m=0\\ m \neq n}}^{N} \frac{1 + |z_m|}{|z_n - z_m|}$$

respectively. Since in our case $z_n = e^{j2\Omega t_{i+n}/N}$ and $\mathcal{K}_\infty(\mathbf{V}_i) = \| \mathbf{V}_i \|_\infty \cdot \| \mathbf{V}_i^{-1} \|_\infty$, the statement of the lemma in (13) follows from simple algebraic manipulations. □

As described in detail in [8], the error in the solution of a Vandermonde system due to parameter inaccuracies can be estimated based on the condition number.

Remark 1: Multiplying both sides of (11) by $\mathbf{V}_i^H$, where the superscript ^{H} stands for conjugate-transposition, transforms (11) into the normal equations

$$\mathbf{V}_i^H \mathbf{V}_i \mathbf{d}_i = \mathbf{V}_i^H \mathbf{D}_i \mathbf{P} \mathbf{q}_i. \tag{15}$$

Since $\mathbf{V}_i^H \mathbf{V}_i$ is a Toeplitz matrix with elements $\sum_{\ell=0}^{N} e^{(m-n)2\Omega t_{i+\ell}/N}$, the above equation is essentially equivalent with the Toeplitz formulation used in [4] and [14]. The representation in (15) offers significant benefit in terms of computational complexity for larger linear systems, when the matrix-vector multiplications in the recursive solution (such as the accelerated conjugate gradient method in [4]) can be sped up by using the FFT algorithm on an augmented circular system. The main disadvantage of this method is that the conditioning of the Toeplitz system can be much worse than that of the Vandermonde system due to the relationship $\mathcal{K}_2(\mathbf{V}_i^H \mathbf{V}_i) = \mathcal{K}_2(\mathbf{V}_i)^2$ between the 2-norm condition numbers [8]. Since we use small matrices, the natural choice is to use the better-conditioned Vandermonde representation.

B. Parameter-Insensitive TDM

In what follows we shall assume that the oscillator in Fig. 3 is described by a periodic orbit in the phase space. Then, the TEM with multiplicative coupling and feedback can be described by the ASDM [15] shown in Fig. 4 where the integrator's time constant κ and the Schmitt-trigger's height b and width δ are the circuit parameters. Since $\delta_{k+1} - \delta_k = 2\kappa\delta$ holds [see (3)–(5)]

$$q_k = \int_{t_k}^{t_{k+1}} u(s) ds = (-1)^k (2\kappa\delta - bT_k). \tag{16}$$

In addition, the bounds for T_k [see also (5)] give

$$\frac{2\kappa\delta}{b+c} \leq T_k \leq \frac{2\kappa\delta}{b-c}$$

and

$$r = \frac{2\kappa\delta}{b-c} \cdot \frac{\Omega}{\pi} < 1 \tag{17}$$

is a sufficient condition for perfect reconstruction [12]. Such TEMs offer a natural way for developing TDMs that are *insensitive* with respect to the TEM circuit parameters. The compensation principle of [12] takes the form

$$q_{k+1} + q_k = \int_{t_k}^{t_{k+2}} u(s) ds = (-1)^k b(T_{k+1} - T_k) \tag{18}$$

for all $k \in \mathbb{Z}$. Note that the right-hand side of equality (18) above does not depend on δ. In addition, an inaccurate value for b merely introduces a constant scaling error in the reconstructed signal. Therefore, any recovery algorithm based on (18), i.e., $q_{k+1} + q_k$, does not have knowledge of the parameters of the TEM and is, thereby, parameter-insensitive.

The TDM coefficients $\mathbf{d}_i$ in (11) directly depend on the circuit parameters b, κ, and δ through $\mathbf{Pq}_i$, since

$[\mathbf{q}_i]_n = (-1)^{i+n}(2\kappa\delta - bT_{i+n})$. We note that the components of $\mathbf{P}\mathbf{q}_i$ are given by [14]

$$[\mathbf{P}\mathbf{q}_i]_n = \kappa\delta[1-(-1)^n] - b\sum_{i=n}^{N}(-1)^i T_i. \tag{19}$$

This expression does not depend on $\kappa\delta$ for even n. For odd n, the terms $\kappa\delta[1-(-1)^n]$ can be eliminated by subtracting from $\mathbf{P}_i$ an appropriate rank-one matrix as detailed below.

Algorithm 2: The Vandermonde system in (11) can be reduced to an underdetermined linear system whose minimum-least-square and minimim-norm solution is given by

$$\mathbf{d}_i = b\left(\mathbf{x}_i - \frac{1}{\alpha_i}\mathbf{y}_i\mathbf{y}_i^H\mathbf{x}_i\right) \tag{20}$$

where $\alpha_i = \mathbf{y}_i^H\mathbf{y}_i$ and, $\mathbf{x}_i$ and $\mathbf{y}_i$ denote the solutions of the Vandermonde systems

$$\mathbf{V}_i\mathbf{x}_i = \mathbf{D}_i(\mathbf{P} - \mathbf{a}\mathbf{b}^H)\mathbf{r}_i \tag{21}$$

and

$$\mathbf{V}_i\mathbf{y}_i = \mathbf{D}_i\mathbf{a}, \tag{22}$$

respectively, where $[\mathbf{r}_i]_n = (-1)^{i+n+1}T_{i+n}$ does not depend $\kappa\delta$, $\mathbf{a}^H = [\ldots,0,1,0,1]$, and $\mathbf{b}^H = [0,\ldots,0,0,1]$.

Proof: The relationship in (19) and the definitions of $\mathbf{a}$, $\mathbf{b}$, and $\mathbf{r}_i$ imply:

$$(\mathbf{P} - \mathbf{a}\mathbf{b}^H)\mathbf{q}_i = b(\mathbf{P} - \mathbf{a}\mathbf{b}^H)\mathbf{r}_i. \tag{23}$$

Denoting the identity matrix of size $N+1$ by $\mathbf{I}$ and using $\mathbf{a}\mathbf{b}^H = \mathbf{a}\mathbf{b}^H\mathbf{P}$, we have $\mathbf{P} - \mathbf{a}\mathbf{b}^H = (\mathbf{I} - \mathbf{a}\mathbf{b}^H)\mathbf{P}$. It is easy to show that $\mathbf{I} - \mathbf{a}\mathbf{b}^H$ is a projection matrix with rank N.

Therefore, by using (23) and (11), we obtain the underdetermined linear system

$$\begin{aligned} b(\mathbf{P} - \mathbf{a}\mathbf{b}^H)\mathbf{r}_i &= (\mathbf{I} - \mathbf{a}\mathbf{b}^H)\mathbf{P}\mathbf{q}_i \\ &= (\mathbf{I} - \mathbf{a}\mathbf{b}^H)\mathbf{D}_i^{-1}\mathbf{V}_i\mathbf{d}_i. \end{aligned}$$

After rearranging terms, we have

$$\left(\mathbf{V}_i + \mathbf{u}_i\mathbf{v}_i^H\right)\mathbf{d}_i = \mathbf{p}_i \tag{24}$$

where $\mathbf{u}_i = -\mathbf{D}_i\mathbf{a}$, $\mathbf{v}_i^H = \mathbf{b}^H\mathbf{D}_i^{-1}\mathbf{V}_i$ and $\mathbf{p}_i = b\mathbf{D}_i(\mathbf{P} - \mathbf{a}\mathbf{b}^H)\mathbf{r}_i$. A minimum-least-square and minimum-norm solution of (24) is given by

$$\mathbf{d}_i = \left(\mathbf{V}_i + \mathbf{u}_i\mathbf{v}_i^H\right)^+\mathbf{p}_i,$$

where the superscript $+$ stands for the pseudo-inverse [8], [2]. Since (24) is a linear system modified by the rank-one matrix $\mathbf{u}_i\mathbf{v}_i^H$, $(\mathbf{V}_i + \mathbf{u}_i\mathbf{v}_i^H)^+$ can be calculated by the general formulas (6 possible cases) presented in [2] (Theorem 3.1.3). Note also that since $\mathbf{V}_i$ is nonsingular and

$$1 + \mathbf{v}_i^H\mathbf{V}_i^{-1}\mathbf{u}_i = 1 - \mathbf{b}^H\mathbf{a} = 0,$$

the corresponding result of [2] (case (vi)) gives (20) after simplifications (and using the fact that $[\mathbf{p}_i]_N = 0$). □

Lemma 2: Algorithm 2 is robust in the sense that division by "very small" α_i is safely avoided and

$$\alpha_i = \mathbf{y}_i^H\mathbf{y}_i \geq \frac{1}{(N+1)^2} \tag{25}$$

for all $i \in \mathbb{Z}$.

Proof: Clearly $\alpha_i = \|\mathbf{y}_i\|_2^2$. Also, $\mathbf{V}_i\mathbf{y}_i = -\mathbf{D}_i^{-1}\mathbf{a}$ implies $\|\mathbf{D}_i^{-1}\mathbf{a}\|_\infty \leq \|\mathbf{V}_i\|_\infty\|\mathbf{y}_i\|_\infty$. Finally, from $\|\mathbf{D}_i^{-1}\mathbf{a}\|_\infty = 1$, (14), and (see [8. p. 53]) $\|\mathbf{V}_i\|_\infty \leq \|\mathbf{V}_i\|_2$, (25) follows. □

As illustrated in the example of Section III-D, for large N numerical inaccuracies might occur if $\|\mathbf{y}_i\mathbf{y}_i^H/\alpha_i\| \gg 1$. Finally, since in the parameter-insensitive case two Vandermonde systems have to be solved, the overall computational load is around $5N^2$ (the rest of the computations in (20) only need $\mathcal{O}(N)$ flops).

C. Error Estimate of the Parameter-Insensitive TDM

As shown above, the coefficients $\mathbf{d}_i$ in (20) are found in the parameter insensitive case by a projection on an N-dimensional subspace of the column space of $\mathbf{V}_i$ (of dimension $N+1$). Therefore, the accuracy of the reconstruction based on (20), (21), and (22) is certainly below that obtained by solving (11) directly.

Lemma 3: The error in the parameter-insensitive case

$$e_i(t) = u(t) - u_i(t) \tag{26}$$

is given by

$$\begin{aligned} e_i(t) = \tilde{e}_i(t) + \beta_i \sum_{n=0}^{N} j \\ \times \left(\Omega - n\frac{2\Omega}{N}\right)[\mathbf{y}_i]_n e^{j(-\Omega + n\frac{2\Omega}{N})t}, \end{aligned} \tag{27}$$

where

$$\beta_i = (2\kappa\delta - bT_{i+N})(-1)^{i+N} + b\frac{\mathbf{y}_i^H\mathbf{x}_i}{\alpha_i}. \tag{28}$$

Proof: Recall that $\tilde{e}_i(t)$ is the error without using the parameter-insensitive formulation [see also (12)]. Then, with $\mathbf{g}^H(t)$ with elements $j(-\Omega + n(2\Omega)/(N))e^{j(\Omega - n(2\Omega)/(N))t}$ we have

$$\tilde{e}_i(t) = u(t) - \mathbf{g}^H(t)\mathbf{d}_i \tag{29}$$

where $\mathbf{d}_i$ is the solution of (11). Likewise, the error in the parameter-insensitive formulation is given by

$$e_i(t) = u(t) - \mathbf{g}^H(t) b \left(\mathbf{x}_i - \frac{\mathbf{y}_i \mathbf{y}_i^H \mathbf{x}_i}{\alpha_i} \right). \tag{30}$$

With (23) and (11), (21) can be rewritten as

$$\begin{aligned} \mathbf{V}_i \mathbf{x}_i &= \mathbf{D}_i (\mathbf{P} - \mathbf{a}\mathbf{b}^H) \mathbf{q}_i / b \\ &= (\mathbf{V}_i \mathbf{d}_i - \mathbf{D}_i \mathbf{a}\mathbf{b}^H \mathbf{q}_i) / b \end{aligned}$$

and therefore, with (22)

$$\begin{aligned} \mathbf{x}_i &= (\mathbf{d}_i - \mathbf{V}_i^{-1} \mathbf{D}_i \mathbf{a}\mathbf{b}^H \mathbf{q}_i) / b \\ &= (\mathbf{d}_i - \mathbf{y}_i \mathbf{b}^H \mathbf{q}_i) / b. \end{aligned}$$

Substituting $\mathbf{x}_i$ above into (30) and using (29) gives

$$e_i(t) = \tilde{e}_i(t) + \left(\mathbf{b}^H \mathbf{q}_i + b \frac{\mathbf{y}_i^H \mathbf{x}_i}{\alpha_i} \right) \mathbf{g}^H(t) \mathbf{y}_i.$$

This concludes the proof. □

Remark 2: Ignoring the term $\tilde{e}_i(t)$ in (27) gives the approximation

$$e_i(t) \simeq \beta_i \sum_{n=0}^{N} j \left(\Omega - n \frac{2\Omega}{N} \right) [\mathbf{y}_i]_n e^{j\left(-\Omega + n \frac{2\Omega}{N}\right) t}. \tag{31}$$

The formula for β_i can be used only when accurate values for $\kappa\delta$ and b are known. Since generally this is not the case, we define the average consecutive error $e_i^{\mathrm{ace}}(t) = (e_i(t) + e_{i+1}(t))/2$. Assuming furthermore that the sum on the right-hand side of (31) is the same for i and $i+1$, the error estimate becomes

$$e_i^{\mathrm{ace}}(t) = \gamma_i \sum_{n=0}^{N} j \left(\Omega - n \frac{2\Omega}{N} \right) [\mathbf{y}_i]_n e^{j\left(-\Omega + n \frac{2\Omega}{N}\right) t} \tag{32}$$

where

$$\gamma_i = \frac{b}{2} \left[(T_{i+N+1} - T_{i+N})(-1)^{i+N} + \frac{\mathbf{y}_i^H \mathbf{x}_i}{\alpha_i} + \frac{\mathbf{y}_{i+1}^H \mathbf{x}_{i+1}}{\alpha_{i+1}} \right]. \tag{33}$$

As the example in Section III below demonstrates, this error estimate gives reasonable results with the additional benefit that the interval-reducing parameter M can also be estimated. Finally, since this error estimate is proportional to b, an accurate value for b is not needed.

D. Example

Here we demonstrate the results above by simulations. The input $u(t)$ to the TEM in Fig. 4 is given by a sum of 100 sinusoids with random amplitudes, phases, and frequencies with an overall bandwidth of 300 Hz ($\Omega = 600\pi$). The input was scaled to satisfy the condition (2) with $c = 0.3$. Fig. 5(a) shows the segment of $u(t)$ we used in the simulations. With parameters $\kappa = 1$ ms, $\delta = 0.17$, and $b = 0.6$, the second inequality in (17) is satisfied with $r = 0.68$. The TEM in Fig. 4 was simulated and 347 trigger times were obtained by recursively solving the equations in (16) with the initial condition $y(t_0) = -\delta$. Fig. 5(b) shows the TEM signals of Fig. 4 in a smaller time range.

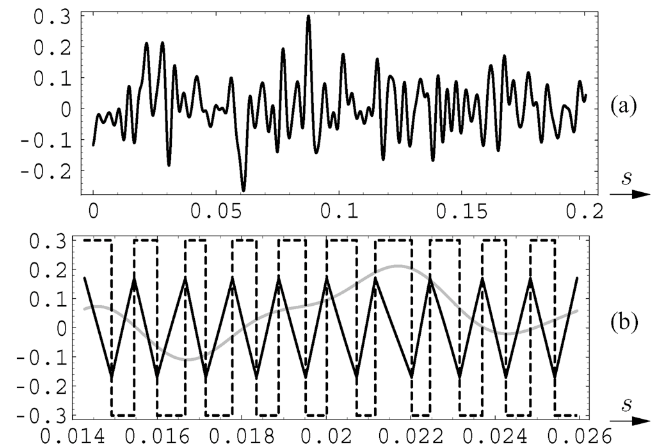

Fig. 5. (a) Input signal as a sum of 100 sinusoids with $\Omega = 2\pi 300$ rad/s. (b) TEM input (gray), integrator output (black), and TEM output (dashed).

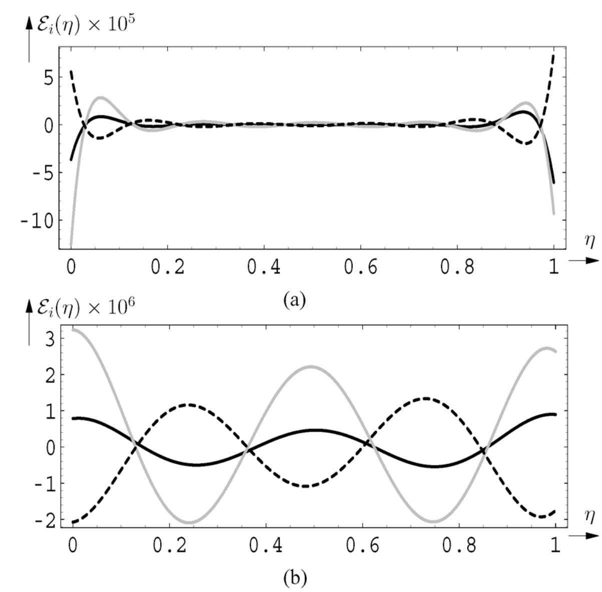

Fig. 6. Scaled and shifted error functions $\mathcal{E}_i(\eta) = e_i(\eta(t_{i+N-M} - t_{i+M}) + t_{i+M})$ with $M = 0$ (a) and $M = 3$ (b) with $i = 10$ (black), $i = 100$ (gray), and $i = 200$ (dashed). The length of the segment is $N = 11$.

The finite dimensional covering was tested for various segments of $u(t)$ in Fig. 5(a). Typical results are shown in Figs. 6 and 7.

Fig. 6 shows the error function $e_i(t)$ for $i = 10, 100, 200$ and $N = 11$ with $M = 0$ in Fig. 6(a) and $M = 3$ in Fig. 6(b). Note that the compact representation in Fig. 6 was made possible by the change of variables $t = \eta \cdot (t_{i+N-M} - t_{i+M}) + t_{i+M}$ on the restricted range $[t_{i+M}, t_{i+M-N}]$ with $\eta \in [0, 1]$.

Fig. 7(a) shows the infinite-norm condition number of $\mathbf{V}_i$ on a log scale and the corresponding upper and lower bounds computed according to (13) as a function of N for $i = 123$.

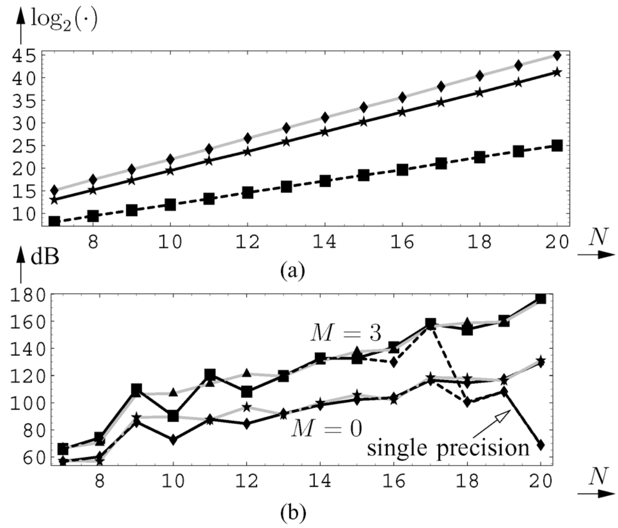

Fig. 7. (a) The infinite-norm condition number of $\mathbf{V}_{123}$ (black) together with the upper (gray) and lower (dashed) bounds. (b) SNR with double and single bit precision in black solid and dashed lines, respectively, and the SNR evaluated using the error estimate in gray.

As mentioned before, by increasing N the conditioning of $\mathbf{V}_i$ gets worse. The quality of the reconstruction quantified as the signal-to-noise ratio (SNR) in dB is given by

$$u^{\mathrm{RMS}} - 10 \lg \left(\frac{1}{t_{i+N-M} - t_{i+M}} \int_{t_{i+M}}^{t_{i+N-M}} e_i^2(t) dt \right),$$

where u^{RMS} denotes the RMS value of $u(t)$ in dB. ($u^{\mathrm{RMS}} = -21.9$ dB in Fig. 5(a)]. The SNR evaluated by using both double and single bit precision is shown in Fig. 7(b) together with those corresponding to the error estimates in (32) in terms of N for $M = 0$ and $M = 3$.

It can be seen, that the error is drastically decreased for larger N by a small increase of M. This result is not surprising given that our approach to approximating $u(t)$ is equivalent to taking the time derivative of a Lagrange interpolation with interpolating points (referred to as nodes) $e^{j2\Omega t_{i+n}/N}$ ($n = 0, 1, \ldots, N$). The large interpolation error at the boundaries of the interpolating interval [see Fig. 7(a)] is due to the well-known Runge phenomenon. Specially placed nodes (such as the Chebyshev nodes) can remedy this problem. However, node placement can not be employed here since the trigger times (and hence the nodes) are input parameters. The remaining option is to set M to some value (usually between 2 and 5) based on the trigger times and the error estimate. Finally, we note that the error traces close to the estimates were calculated with double bit precision. The dashed error traces were obtained with the built-in single bit precision. For $N > 17$ the extra error is due to numerical inaccuracies arising in the subtraction in (20). Therefore, selecting the condition number, shown as a function of N in Fig. 7(a), is an important design choice.

Remark 3: Because of boundary effects, the TEM investigated above operates with an oversampling ratio (or OSR defined as the Nyquist period π/Ω divided by the average of the T_k's), between 2 and 3. This is a radically different mode of operation than that of synchronous sigma-delta modulators whose typical OSR is in the several hundreds [18]. In contrast to conventional synchronous sigma-delta modulators, the ASDM-based TEM investigated here does not exhibit the "noise shaping" property if the time quantizer is outside the feedback loop. If the time quantizer is in the feedback loop, a first order noise shaping effect is discernable for high OSRs. Since the OSR needs to be in the several hundreds in order to create a noticeable noise shaping effect, however, noise shaping is hardly relevant in our setting.

IV. Stitching Algorithm for Signal Recovery

A. Stitching Algorithm

Since excellent approximations can be achieved within finite time intervals (see Section III-D), a reasonable approach for the overall reconstruction of the input signal $u(t)$ on the real line is to (i) carry out approximations in different intervals using the formulation in Section III, (ii) cut out the accurate parts by appropriate windows with finite support in the time domain and forming a partition of unity, (iii) sum up the windowed approximations, and finally (iv) carry out efficient post-processing.

Several window types are available in the literature (such as those used in Wavelet theory) that do not dependent on the trigger times. Since, N is a key parameter in terms of both conditioning and accuracy (see Fig. 7), the use of variable windows determined by trigger times seems to be a natural choice in our setting. As explained below, adjacent windows should overlap over a certain number of trigger times. The number of trigger times that overlap in adjacent windows will be subsequently denoted by K. Using the notation

$$\begin{aligned} J &= N - 2M - K, \\ \tau_n &= t_{nJ+M}, \\ \sigma_n &= t_{nJ+M+K} \end{aligned} \tag{34}$$

we define the windows

$$w_n(t) = \begin{cases} 0 & \text{if } t \notin (\tau_n, \sigma_{n+1}], \\ \theta_n(t) & \text{if } t \in (\tau_n, \sigma_n], \\ 1 & \text{if } t \in (\sigma_n, \tau_{n+1}], \\ 1 - \theta_{n+1}(t) & \text{if } t \in (\tau_{n+1}, \sigma_{n+1}] \end{cases} \tag{35}$$

where the $\theta_n(t)$'s are appropriately chosen functions. With $t_0 = 0$, $N = 8$, $M = 2$, and $K = 1$ (hence $J = 3$) an illustration is shown in Fig. 8. The lowest trace demonstrates that the windows so defined form a partition of unity.

By stitching the finite dimensional coverings together a natural approximation of the bandlimited signal $u = u(t), t \in \mathbb{R}$, is given by

$$\hat{u}(t) = \sum_{n \in \mathbb{Z}} w_n(t) u_{nJ}(t). \tag{36}$$

It only remains to perform the post-processing operation. In what follows our goal is to calculate the samples of the reconstructed signal $\hat{u}(t)$ taken uniformly with appropriate sampling period S. In this way the reconstructed signal can be processed by standard digital algorithms.

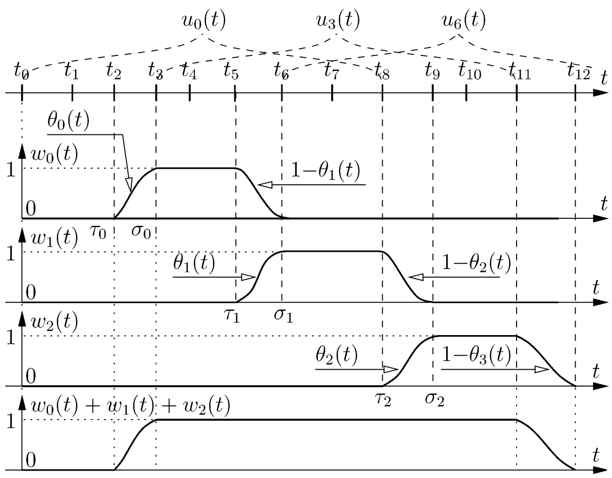

Fig. 8. Illustration of the windows defined in (35) with $t_0 = 0$, $N = 8$, $M = 2$, and $K = 1$.

Since the windows $w_n(t), n \in \mathbb{Z}$, have finite support, $\hat{u}(t)$ in (36) is very well suited for real-time uniform sampling in an overlap-add fashion (see also Fig. 8). In addition, the Fourier-series representation of the finite dimensional coverings in (10) allows calculating the samples $u_{nJ}(kS)$ via the FFT (see Section V). The bandwidth of $\hat{u}(t)$ determines the values of the sampling time S that avoids (or minimizes) aliasing. In particular, denoting the Fourier transform of $w_n(t)$ by $W_n(\omega)$, let ν be such that $W_n(\omega) \simeq 0$ for all $|\omega| > \nu$ and $n \in \mathbb{Z}$. Since the bandwidth of $u_{nJ}(t)$ is Ω [see (10)], the bandwidth of the product $u_{nJ}(t)w_n(t)$ in (36), and thus that of $\hat{u}(t)$ is $\Omega + \nu$. Therefore, for

$$S \leq \frac{\pi}{\Omega + \nu} \tag{37}$$

aliasing is (practically) avoided.

Algorithm 3: The reconstructed signal in discrete-time (DT) is given by $\hat{u}(kS) * h[k]$, where the $h[k]$ is the impulse response of a DT LPF with (digital) cutoff frequency $\pi/(1+\nu/\Omega)$ and $*$ denotes the convolution.

Since the reconstruction error spreads over the range $\omega \in (-\Omega-\nu, \Omega+\nu)$, low-pass filtering further improves the overall accuracy. In addition, the Nyquist rate of the samples can be recovered via decimating the filtered reconstructed samples. However, it depends on the application if an (even accurate) approximation of the filtered samples $u(kS) * h[k]$ is acceptable instead of approximating the original samples $u(kS)$.

Remark 4: Increasing N not only improves the accuracy of the reconstruction [see Fig. 7(b)], but also broadens $w_n(t)$ in the time domain, and hence decreases ν. This technique clearly has its limitations since by increasing N, the condition number of the Vandermonde systems also increases [see Fig. 7(a)]. By appropriately choosing the parameter K and $\theta_n(t)$ in (35), ν can be decreased for fixed N and M. For example, a good frequency localization for $W_n(\omega)$ can be achieved by using

$$\theta_n(t) = \sin^2\left(\frac{\pi}{2} \cdot \frac{t-\tau_n}{\sigma_n - \tau_n}\right) \tag{38}$$

while both $w_n(t)$ and its derivative are continuous.

B. Overall Error Estimation

The DT reconstruction error is given by

$$e[k] = u(kS) - \hat{u}(kS) \tag{39}$$

and if filtering is used the error amounts to

$$\begin{aligned}\tilde{e}[k] &= u(kS) * h[k] - \hat{u}(kS) * h[k] \\ &= e[k] * h[k].\end{aligned} \tag{40}$$

Lemma 4: The DT reconstruction estimated error amounts to

$$e^{\text{ace}}[k] = \sum_{n\in\mathbb{Z}} w_n(kS) e^{\text{ace}}_{nJ}(kS) \tag{41}$$

where e^{ace}_{nJ} is given by (32).

Proof: Since $w_n(t), n \in \mathbb{Z}$, forms a partition of unity, using (36) and (26) the overall reconstruction error $e(t) = u(t) - \hat{u}(t)$ can be written as

$$\begin{aligned}e(t) &= u(t)\sum_{n\in\mathbb{Z}} w_n(t) - \hat{u}(t) \\ &= \sum_{n\in\mathbb{Z}} w_n(t)(u(t) - u_{nJ}(t)) \\ &= \sum_{n\in\mathbb{Z}} w_n(t) e_{nJ}(t).\end{aligned}$$

Approximating $e_{nJ}(t)$ by $e^{\text{ace}}_{nJ}(t)$ and setting $t = kS$, the result follows. □

Remark 5: If postfiltering is employed, then the filtered error estimation sequence

$$e^{\text{ace}}[k] = e^{\text{ace}}[k] * h[k] \tag{42}$$

can be used.

The error estimates in (41) and (42) assume accurate values for the trigger times. In practice the trigger times certainly exhibit jitter as a result of the TEM circuit imperfections [10] and the unavoidable quantization of the T_k's. The jitter-induced error often dominates the reconstruction error obtained with perfect trigger times. Modeling the jitter as a sequence of independent random variables uniformly distributed within $[-\Delta/2, \Delta/2]$ with given Δ, the error estimate (defined in [dB])

$$10\lg\left(\frac{c^2(1-c^2)^2}{3}\right) - 20\lg(2)\log_2(\sigma) - 10\lg(\rho) \tag{43}$$

was developed in [12] for the ideal TDM of Section II-B, with $\sigma = (\max_k T_k - \min_k T_k)/\Delta$ and $\rho = (2\pi/(\max_k T_k + \min_k T_k)/\Omega$. As demonstrated in the example of Section IV-C below, this rough estimate gives acceptable results for the proposed TDM, although the jitter-processing mechanism in this paper is not exactly the same as the one in [12]. The behavior of the error estimate in (41) with corrupted trigger times is rather important. Since the error estimate does not incorporate knowledge about jitter, it relies on the existence of an input that exactly generates the available trigger times. Because of this built-in "tolerance," the error estimate saturates for larger values of N

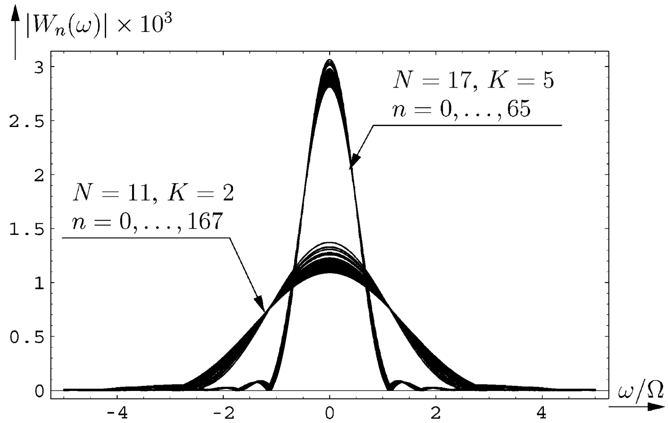

Fig. 9. Two sets of frequency-domain windows with $M = 3$.

than the actual error. As illustrated in Section IV-C, this fact together with (43) makes it possible to determine N for a given Δ. The error estimate eventually also breaks down for large enough N, when "it turns out" that the corrupted trigger times cannot belong to a bandlimited signal. However, at this point N is already determined.

C. Example

In this section, we use the input signal $u(t)$, the TEM parameters and the trigger times of the example in Section III.D. The overall reconstruction was carried out with two sets of window functions, $w_n(t)$ with $N = 11, M = 3, K = 2$ and $N = 17, M = 3, K = 5$, respectively, with $\theta_n(t)$ defined by (38). Fig. 9 shows that the window's Fourier transforms exhibit little variation as a function of n. Using this figure and (37)

$$S = \frac{\pi}{6\Omega} = 277.78\ \mu\text{s}$$

is a safe choice for the sampling period.

For DT postfiltering, a standard Parks-McClellan finite-impulse-response (FIR) low-pass filter of order 153 was designed with passband ripple 1 dB, stopband attenuation 90 dB, passband edge $\pi/6$ and transition band $\pi/25$ [17]. Fig. 10 shows a small portion of the original and the filtered input sequences. To compensate for the delay introduced by the (linear phase) filter, a shifted version of the latter is shown. In this example, we assume that the "distortion" due to the filter is acceptable. The DT reconstruction error $e[k]$ and the corresponding SNR in dB amounts to

$$\text{SNR} = u^{\text{RMS}} - 10\lg\left(\frac{\sum_{k=K\min}^{K\max} e^2[k]}{K_{\max} - K_{\min} + 1}\right) \tag{44}$$

where $u^{\text{RMS}} = -21.9$ dB, $K_{\min}$ and $K_{\max} > K_{\min}$ are appropriate integers. In calculating SNR according to the (40) above, $K_{\min}$ and $K_{\max}$ have to be chosen such that the range $[K_{\min}, K_{\max}]$ excludes the error due to the first and last windows (see the lowest trace of Fig. 8). The reconstructed samples are compared with the filtered input sequence, that is, the error sequence $\tilde{e}[k]$ and the corresponding SNR (denoted by $\widetilde{\text{SNR}}$)

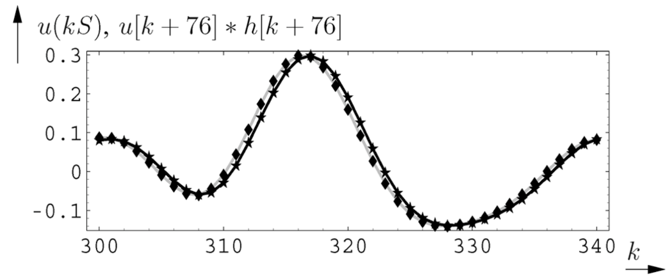

Fig. 10. Small portions of the original input sequence $u(kS)$ (gray) and a delayed filtered sequence.

are evaluated. For evaluating $\widetilde{\text{SNR}}$, $K_{\min}$ and $K_{\max}$ [see (44)] are chosen such that the range $[K_{\min}, K_{\max}]$ excludes the errors due to both the first and last windows, and the filter transient. Finally, the SNR value computed using the $\tilde{e}^{\text{ace}}[k]$ error sequence is denoted by $\widetilde{\text{SNR}}^{\text{ace}}$.

Corresponding to the two sets of windows, portions of the reconstructed and estimated error sequences without and with postfiltering calculated by (39), (40), (41), and (42), as well as the corresponding SNR values evaluated by (44) are shown in Fig. 11. As seen, the improvement due to postfiltering is noticeable, and the overall error estimates are reliable.

Finally we consider the case when the T_k's are corrupted by jitter. In the simulations random numbers uniformly distributed within $[-\Delta/2, \Delta/2]$ were generated with

$$\Delta = 1.1333 \times 10^{-9}$$

and added to the accurate T_k's.

For simplicity, the SNR values evaluated using several error estimates are shown without postfiltering in Fig. 12. The figure indicates the equations used to compute the SNR values. As seen, the SNR computed using (39) saturates for $N \geq 12$. Although (43) underestimates the SNR by about 6–8 dB, its intersection with the trace corresponding to (41) points to N between 12 and 13. The dashed traces correspond to the SNR and its estimated value using the consecutive error formula in (41) without jitter. This confirms, again, that for accurate trigger times the estimate in (41) is reliable. As a result, based on the jitter-corrupted trigger times, parameter c, and Δ, a reconstruction error around -108 dB is predicted for (conservatively chosen) $N = 13$. As shown, this forecast is close to the actual error trace.

V. Practical Computational Considerations

In this section, we demonstrate how overflow can be avoided in the reconstruction algorithms and provide an estimate of the total number of flops needed to implement the stitching algorithm in real-time.

A. Reconstruction Based on the T_k's

Since the t_k's form a strictly increasing sequence of k, a practical reconstruction algorithm cannot use these values because of potential overflow. However, the T_k's are bounded by π/Ω [see (5)]. Our goal in this subsection is to demonstrate a reconstruction algorithm that only uses the T_k's.

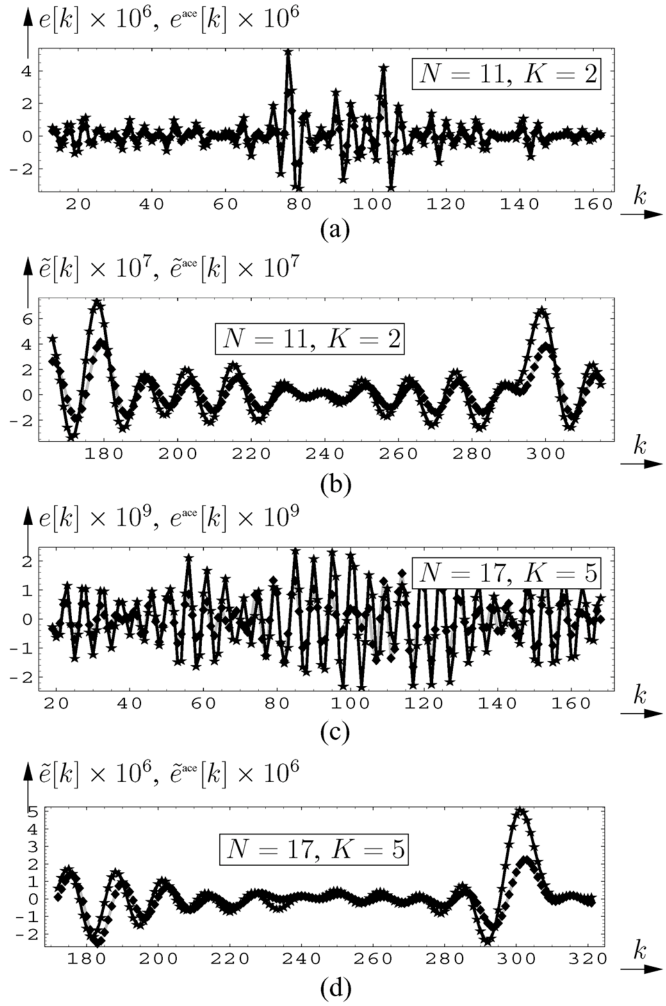

Fig. 11. Error sequences (stars) and average consecutive error sequences (diamonds) without (a,c) and with (b,d) postfiltering for $M = 3$. In the subfigures (a) to (d) $\mathrm{SNR} = 105$ dB, 116 dB, 159 dB, 180 dB, and $\mathrm{SNR}^{ace} = 100$ dB, 112 dB, 154 dB, 175 dB, respectively.

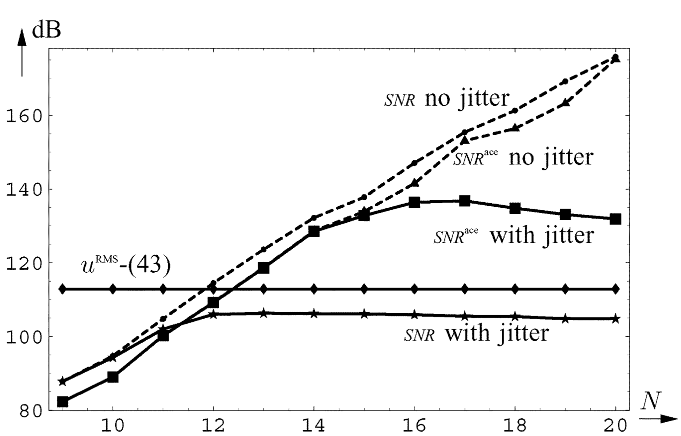

Fig. 12. SNR values evaluated using the error sequences given in (39) and (41) with and without jitter and the rough SNR estimate given in (43).

The samples of the windows employed can easily be generated without using large sampling times. Since $w_n(t) = 0$ for $t \le \tau_n$, where τ_n is monotonically increasing with n [see Fig. 8 and (34)], the first sample occurs at $\lceil \tau_n/S \rceil$ where $\lceil\ \rceil$ stands for the ceiling operation. For a window shifted towards the origin as $w_n(t + l_n S)$, for an appropriate positive integer l_n, we have $w_n(t + l_n S) = 0$ for $t + l_n S \le \tau_n$, i.e., for $t \le \tau_n - l_n S$. The first sample of the shifted window occurs at $\lceil (\tau_n - l_n S)/S \rceil$ and $w_n(\lceil \tau_n/S \rceil) = w_n(\lceil (\tau_n - l_n S)/S \rceil)$ obviously holds. As a result, window samples can be generated by using a bounded set of independent variables after shifting the window close to the origin by appropriate integer multiples of the (given) sampling period.

As for the matrix parameters in the finite-dimensional coverings, no problem arise with the $\mathbf{r}_i$'s. The $\mathbf{D}_i$'s and the $\mathbf{V}_i$'s are determined, on the other hand, by the trigger times through $e^{-j\Omega t_{i+n}}$ and $e^{jm2\Omega t_{i+n}/N}$, respectively. Using the periodicity of the complex exponentials we have $e^{-j\Omega t_{i+n}} = e^{-j\Omega t_{i+n} + M_{i,n} 2\pi}$ and $e^{jm2\Omega t_{i+n}/N} = e^{jm2\Omega t_{i+n}/N - K_{i,m,n} 2\pi}$, where $M_{i,n}$ and $K_{i,m,n}$ are arbitrary integers. Choosing $M_{i,n}$ and $K_{i,m,n}$ appropriately, the exponentials can be generated by a bounded set of quantities.

B. An Estimate of the Total Number of Flops

We have seen that $5N^2$ floating point operations are needed in the parameter-insensitive case for the implementation of a finite-dimensional TDM algorithm. A factor that should be also taken into account comes from generating the samples of (10). Selecting S as

$$S = \frac{\pi}{I\Omega}$$

with an appropriate positive integer I ($I = 6$ in Section IV.C), the samples of (10) can be expressed as

$$u_i(kS) = e^{-jk\frac{\pi}{I}} \sum_{n=0}^{NI-1} \hat{d}_{i,n} e^{jnk\frac{2\pi}{NI}},$$

where $\hat{d}_{i,n} = j(\Omega - n(2\Omega)/(N))d_{i,n}$ if $n \le N$ and $\hat{d}_{i,n} = 0$ if $N < n \le NI - 1$. The summation can be calculated by FFT with $5NI \log_2 NI$ floating point operatins [8]. The rest of the computation requirements includes $\mathcal{O}(N)$ operations and the generation of the complex exponentials. Ignoring these, the dominant number of floating point operations per window becomes

$$5N^2 + 5NI \log_2 NI. \tag{45}$$

Assume finally that the overall range is covered by L windows with $\tau_0 = t_M$, where L is a large integer. The support of the Lth (last) window terminates at σ_{L+1} [see (35)]. Therefore, the total range becomes $\sigma_{L+1} - \tau_0 = t_{(L+1)J+M+K} - t_M$ [see (34)]. Let the average of the T_k's be denoted by R. Then $t_k \simeq kR$, and therefore by using (45) and $J = N - 2M - K$ [see (34)], for large L the number of flops becomes

$$L\frac{5N^2 + 5NI \log_2 NI}{((L+1)J + K)R} \simeq \frac{5N^2 + 5NI \log_2 NI}{(N - 2M - K)R}.$$

Finally, as in [12], R can be approximated by the arithmetic mean of the lower and upper bound for T_k in (17) as $R \simeq (2\kappa\delta/(b-c) + 2\kappa\delta/(b+c))/2$. Using the expression for r in (17)

$$R \simeq \frac{r\pi}{\Omega(1+c/b)}.$$

easily follows. Therefore, we have the following

Lemma 5: The number of flops for realizing the stitching algorithm is given by

$$\frac{5}{r} \cdot \left(1 + \frac{c}{b}\right) \cdot \frac{\Omega}{\pi} \cdot N + \mathcal{O}(N).$$

VI. Conclusion

We investigated the implementation of a signal recovery algorithm that consists of an overlapping sequence of finite-dimensional coverings of an infinite-dimensional space. The recovery of the signal on finite dimensional coverings calls for solving a Vandermonde system.

The main focus of our work was on developing efficient parameter-insensitve TDM algorithms that can be implemented in real-time and that are stable. In order to construct such algorithms, we have developed a novel solution method that calls for projecting the $N+1$-dimensional space generated by the column of the Vandermonde matrix onto N dimensional space. The algorithm was shown to be provably stable.

The real-time algorithm stitches finite-dimensional coverings together using a set of variable-size windows that are data driven. A linear filtering of the output of the real-time algorithm further improves its performance. The complexity of the stitching algorithm is linear in size of the finite-dimensional coverings. It is, therefore, amenable to real-time implementations.

Currently, we are evaluating the stitching algorithm described here in experimental body area networks. The stringent energy constraints at the transmitter (sensor) side can be addressed by using ultrawide-wide-band wireless communication channels [19] or the skin surface as a communication medium [9]. The trigger times can be readily transmitted through either of these channels while the decoding complexity can be easily implemented at the receiver.

Acknowledgment

The authors would like to thank two of the reviewers for both carefully reading the paper and making detailed suggestions for improving its presentation.

References

[1] A. Björk and V. Pereyra, "Solution of Vandermonde systems of equations," *Math. Comp.*, vol. 24, pp. 893–903, 1970.

[2] S. L. Campbell and C. D. Meyer Jr:, *Generalized Inverses of Linear Transformations*. New York: Dove, 1979.

[3] O. Christensen, "Frames Riesz basis, and discrete Gabor/wavelet expansions," in *Bull. Amer. Math. Soc.*, Mar. 27, 2001, vol. 38, no. 3, pp. 273–291.

[4] H. G. Feichtinger, K. Gröchenig, and T. Strohmer, "Efficient numerical methods in non-uniform sampling theory," *Numer. Math.*, vol. 69, pp. 423–440, 1995.

[5] H. G. Feichtinger and T. Werther, "Improved locality for irregular sampling algorithms," in *Proc. ICASSP*, Istanbul, Turkey, 2000.

[6] W. Gautschi, "Norm estimates for the inverses of Vandermonde matrices," *Numer. Math.*, vol. 23, pp. 337–347, 1975.

[7] W. Gautschi, "On the inverses of vandermonde and confluent vandermonde matrices," *Numer. Math.*, vol. 29, pp. 445–450, 1978.

[8] G. H. Golub and C. F. Van Loan*, Matrix Computations*, 3rd ed. Baltimore, MD: The John Hopkins University Press, 1996.

[9] C. Káldi, A. A. Lazar, E. K. Simonyi, and L. T. Tóth, "Time Encoded Communications for Human Area Network Biomonitoring," Department of Elec. Eng., Columbia University, New York, BNET Tech. Rep.#2-07, Jun. 2007.

[10] P. R. Kinget, A. A. Lazar, and L. T. Tóth, "On the robustness of an analog VLSI implementation of a time encoding machine," in *Proc. ISCAS*, Kobe, Japan, May 23–26, 2005, pp. 4221–4224.

[11] J. Kovačević, P. L. Dragotti, and V. K. Goyal, "Filter bank frame expansions with erasures, invited paper," *IEEE Trans. Inf. Theory*, vol. 48, no. 6, pp. 1439–1450, Jun. 2002.

[12] A. A. Lazar and L. T. Tóth, "Perfect recovery and sensitivity analysis of time encoded bandlimited signals," *IEEE Trans. Circuits Syst. I, Reg. Papers*, vol. 51, no. 10, pp. 2060–2073, Oct. 2004.

[13] A. A. Lazar, "Time encoding with an integrate-and-fire neuron with a refractory period," *Neurocomput.*, vol. 58–60, pp. 53–58, 2004.

[14] A. A. Lazar, E. K. Simonyi, and L. T. Tóth, "Fast recovery algorithms of time encoded bandlimited signals," in *Proc ICASSP*, Philadelphia, PA, Mar. 19–23, 2005, vol. 4, pp. 237–240, 2005.

[15] A. A. Lazar, "Time encoding machines with multiplicative coupling, feedforward and feedback," *IEEE Trans. Circuits Syst. II, Exp. Briefs*, vol. 53, no. 8, pp. 672–676, Aug. 2006.

[16] A. A. Lazar, E. K. Simonyi, and L. T. Tóth, "A real-time algorithm for time decoding machines," in *Proc. 14th Eur. Signal Process. Conf.* , Florence, Italy, Sep. 4–8, 2006.

[17] Parks-McClellan FIR Filter Design [Online]. Available: http://www.dsptutor.freeuk.com/remez/RemezFIRFilterDesign.html Java 1.1 Version

[18] E. Roza, "Analog-to-digital conversion via duty-cycle modulation," *IEEE Trans. Circuits Syst. II, Analog Digit. Signal Process.*, vol. 44, no. 11, pp. 907–917, Nov. 1997.

[19] J. Ryckaert, C. Desset, A. Fort, M. Badaroglu, V. De Heyn, P. Wambacq, G. Van der Plas, S. Donnay, B. Van Poucke, and B. Gyselinckx, "Ultra-wide-band transmitter for low-power wireless body area networks: Design and evaluation," *IEEE Trans. Circuits Syst. I, Reg. Papers*, vol. 52, no. 12, pp. 2515–2525, Dec. 2005.

[20] T. Strohmer, "Irregular Sampling, Frames, and Pseudoinverse," Master thesis, Dep. Math. , Univ. Vienna, Vienna, Austria, 1991.

[21] T. Strohmer, "Numerical analysis of the non-uniform sampling problem," *J. Comput. Appl. Math.*, vol. 122, pp. 297–316, 2000.

Aurel A. Lazar is a Professor of Electrical Engineering at Columbia University, New York. In the mid 1980s and 1990s, he pioneered investigations into networking games and programmable networks. In addition, he conducted research in broadband networking with quality of service constraints; and in architectures, network management and control of telecommunications networks. His current research interests are at the intersection of Computational Neuroscience, Information/Communications Theory and Systems Biology. In silico, his focus is on time encoding and information representation in sensory systems, and, spike processing and neural computation in the cortex. In vivo, his focus is on the olfactory system of the drosophila.

Ernö K. Simonyi received the M.Sc. and the University Doctor degrees both in electrical engineering from the Technical University of Budapest (BME) in 1968 and 1974, respectively, the Candidate's (Ph.D.) degree in microelectronics from the Hungarian Academy of Sciences, Budapest, Hungary, in 1980.

Since 1984 he has been with BME as Titular University Associate Professor. He joined the Research Institute for Telecommunications (TKI) in 1968. Throughout 1978 he was with the University of California, Los Angeles. From 1982 till 1990 he was the head of Signal Processing & Computer Science Department in TKI. In 1991–1992 he was the Deputy General Director of the TKI. From 1993 till 2008 he was the Managing Director of his own consulting firms specializing on large nationwide ICT projects. Since 2005 he has been with Ministry of Defence Electronics, Logistics and Property Management Co.

Dr. Simonyi was the Editor-in-Chief of the *Journal of Communications* (Hiradástechnika) during 1998–2000. During 2001–2004, he was the President of the National Council of Hungary for Information and Communications Technology.

László T. Tóth received the M.S. degree in 1982 from the Technical University of Budapest, Hungary, the Habilitation degree from the Budapest University of Technology and Economics,Budapest, Hungary, in 2005, and the Candidate's (Ph.D.) and D.Sc. degrees from Hungarian Academy of Sciences, Budapest, Hungary, in 1987 and 2005, respectively.

He worked for the Research Institute for Telecommunications (1982–93, Budapest, Hungary), Bell Laboratories (1996–1997, Murray Hill, NJ, USA), and Columbia University (1989–90, 1995–96). He taught at the Technical University of Budapest (1993–99) and Columbia University (1999–2002). Currently he is a Full Professor at the Department of Telecommunications and Media Informatics, Budapest University of Technology and Economics, Hungary.

Dr. Tóth was an Associate Editor of the *Journal of Communications* (Hiradástechnika, 1998–2000) and the IEEE TRANSACTIONS ON CIRCUITS AND SYSTEMS—II: ANALOG DIGITAL SIGNAL PROCESSING (1999–2002).